High Performance Organic Photovoltaics with Plasmonic-Coupled Metal Nanoparticle Clusters

Hyung Il Park,[†,§,⊥] Seunghoon Lee,[‡,§,⊥] Ju Min Lee,[†,§] Soo Ah Nam,[†,§] Taewoo Jeon,[†,§] Sang Woo Han,[*,‡,§] and Sang Ouk Kim[*,†,§]

[†]Department of Materials Science and Engineering, KAIST, Daejeon 305-701, Republic of Korea, [‡]Department of Chemistry and KI for the NanoCentury, KAIST, Daejeon 305-701, Republic of Korea, and [§]Center for Nanomaterials and Chemical Reactions, Institute for Basic Science (IBS), Daejeon 305-701, Republic of Korea. [⊥]H. I. Park and S. Lee contributed equally.

ABSTRACT Performance enhancement of organic photovoltaics using plasmonic nanoparticles has been limited without interparticle plasmon coupling. We demonstrate high performance organic photovoltaics employing gold nanoparticle clusters with controlled morphology as a plasmonic component. Near-field coupling at the interparticle gaps of nanoparticle clusters gives rise to strong enhancement in localized electromagnetic field, which led to the significant improvement of exciton generation and dissociation in the active layer of organic solar cells. A power conversion efficiency of 9.48% is attained by employing gold nanoparticle clusters at the bottom of the organic active layer. This is one of the highest efficiency values reported thus far for the single active layer organic photovoltaics.

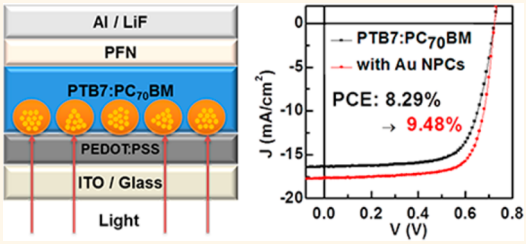

KEYWORDS: organic photovoltaics · cluster · plasmon · electric field distribution · exciton dissociation

Organic photovoltaics (OPVs) are renewable energy conversion devices with distinct potential advantages, such as solution processability, mechanical flexibility, and light weight.[1−5] Over the past decades, enormous research efforts have been devoted to improve the device performances of OPVs by synthesizing new organic semiconductors,[6−12] morphological optimization of organic active layer and developing new device architectures.[13−31] Despite noticeable success in the different approaches, the power conversion efficiency (PCE) of OPV still reveals a large room for improvement due to the inherent drawbacks, such as poor light absorption, short exciton diffusion length, and low carrier mobility in the organic active layers.[20,32−35]

Metal nanoparticles (NPs) with localized surface plasmon resonance (LSPR) have attracted tremendous research interest for the effective enhancement of light absorption and charge generation of OPVs.[27,35−51] To date, light absorption characteristics of OPVs have been widely explored by tuning the size, shape, component, and dielectric environment of plasmonic NPs. Light scattering and near-field enhancement effects at the plasmonic NPs are principal mechanisms for the improved light absorption. The scattering at NPs increases optical path length and, thus, effectively confine light propagation within the organic active layer, resulting in a promoted exciton generation.[36−44] Concurrently, local enhancement of electromagnetic field by the plasmonic NPs can facilitate exciton dissociation.[48−58] Presently, plasmonic NPs are principally located in the charge transport layers or electrodes of OPVs to avoid unnecessary charge trap or device short. As typical OPV active layer thickness is 80−100 nm, commonly employed 40−80 nm size NPs for visible absorption spectrum commonly may cause undesirable exciton quenching/trap or device short within the active layer. In this geometry, however, the spatial separation between NPs and active layer is generally considered less effective for device performance optimization.[59] Moreover, the random spatial arrangement and uncontrolled aggregation of NPs hardly exploit the localized plasmonic enhancement by interparticle coupling.

* Address correspondence to sangouk.kim@kaist.ac.kr, sangwoohan@kaist.ac.kr.

Received for review June 27, 2014 and accepted October 9, 2014.

Published online October 09, 2014
10.1021/nn503508p

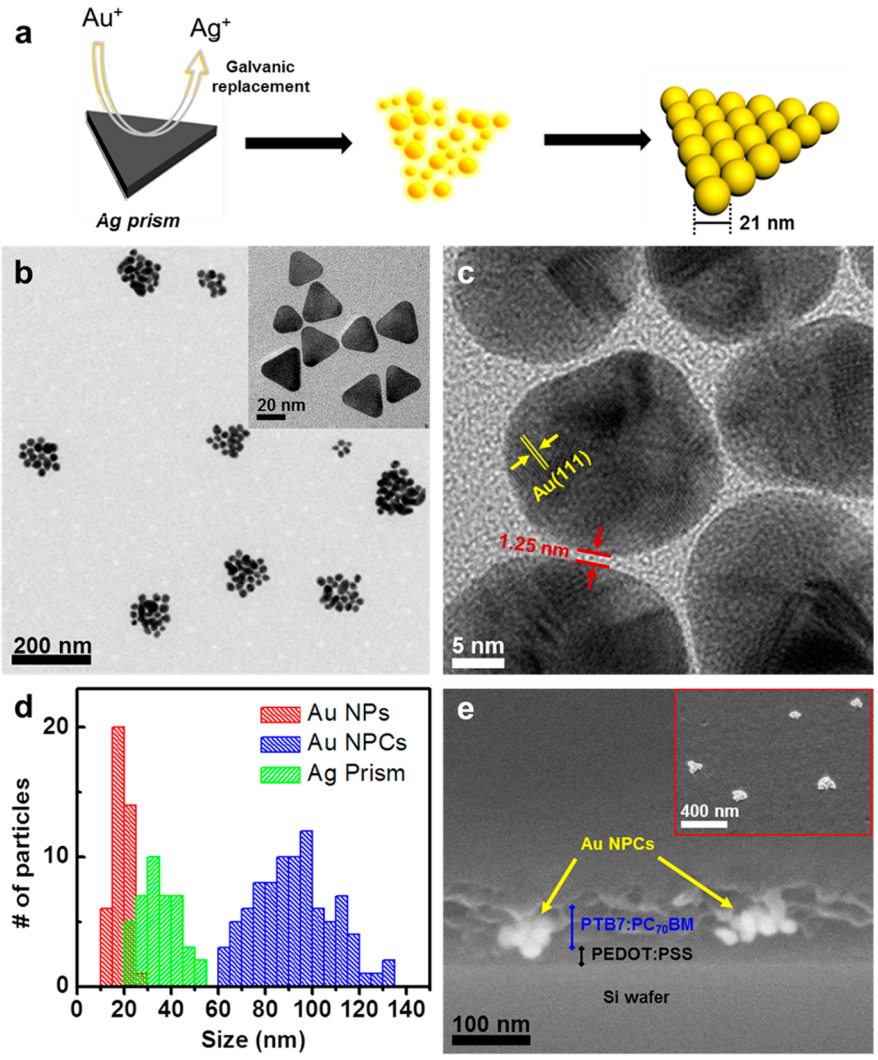

Figure 1. (a) Schematic synthesis procedure of Au NPCs. (b) TEM images of Au NPCs and Ag nanoprisms. (c) High-magnification TEM image of Au NPCs. (d) Size distribution of Au NPs, NPCs, and Ag nanoprisms. (e) Cross-sectional SEM image of Si/PEDOT:PSS/Au NPCs/PTB7:$PC_{70}BM$ layer and tilted-view SEM image of Au NPC layers spin-coated onto PEDOT:PSS film.

In this work, we demonstrate high performance OPVs with Au NP clusters (NPCs) directly incorporated at the bottom of organic active layer. Triangle-shaped Au NPCs consisting of laterally assembled small Au NPs (mean diameter: 21 nm) were synthesized *via* galvanic replacement of Ag nanoprisms with Au precursors. Such nanoscale platelike NPCs could be incorporated at the bottom of organic active layer without significant concern for device short. Owing to the near-field coupling at the interparticle gaps, NPCs can give rise to much broader LSPR absorption and enhanced electric field compared to conventional Au NPs. Consequently, both exciton generation and dissociation are remarkably enhanced in the bulk-heterojunction active layer of OPVs consisting of PTB7 and $PC_{70}BM$. PCE of 9.48% is achieved for the single active layer OPV.

RESULTS AND DISCUSSION

Figure 1a schematically describes the synthetic procedure for Au NPC preparation.[60] Ag nanoprisms were employed as sacrificial templates for galvanic replacement into Au NPCs. Transmission electron microscopy (TEM) image of the synthesized NPCs is shown in Figure 1b. Ag nanoprisms are contrasted in the inset. Each triangular NPC is laterally assembled from Au NPs with the interparticle spacing of 0.5−2 nm (Figure 1c). Size distribution histogram (Figure 1d) reveals that NPCs of 97 ± 25 nm lateral size were synthesized from 34 ± 8 nm size nanoprisms. The typical size of NPs constituting NPCs was 21 ± 3 nm. Figure 1e shows the cross-sectional scanning electron microscopy (SEM) image of Au NPCs embedded between the hole transport layer (poly(3,4-ethylenedioxythiophene):polystyrene sulfonic acid, PEDOT:PSS) and the organic active layer, which is the bulk-heterojunctions of poly[[4,8-bis[(2-ethylhexyl)oxy]benzo[1,2-*b*:4,5-*b*′]dithiophene-2,6-diyl][3-fluoro-2-[(2-ethylhexyl)-carbonyl]-thieno-[3,4-*b*]thiophenediyl]] (PTB7, electron donor) and [6,6]-phenyl-C_{70} butyric acid methyl ester ($PC_{70}BM$, electron acceptor). For the maximized near-field

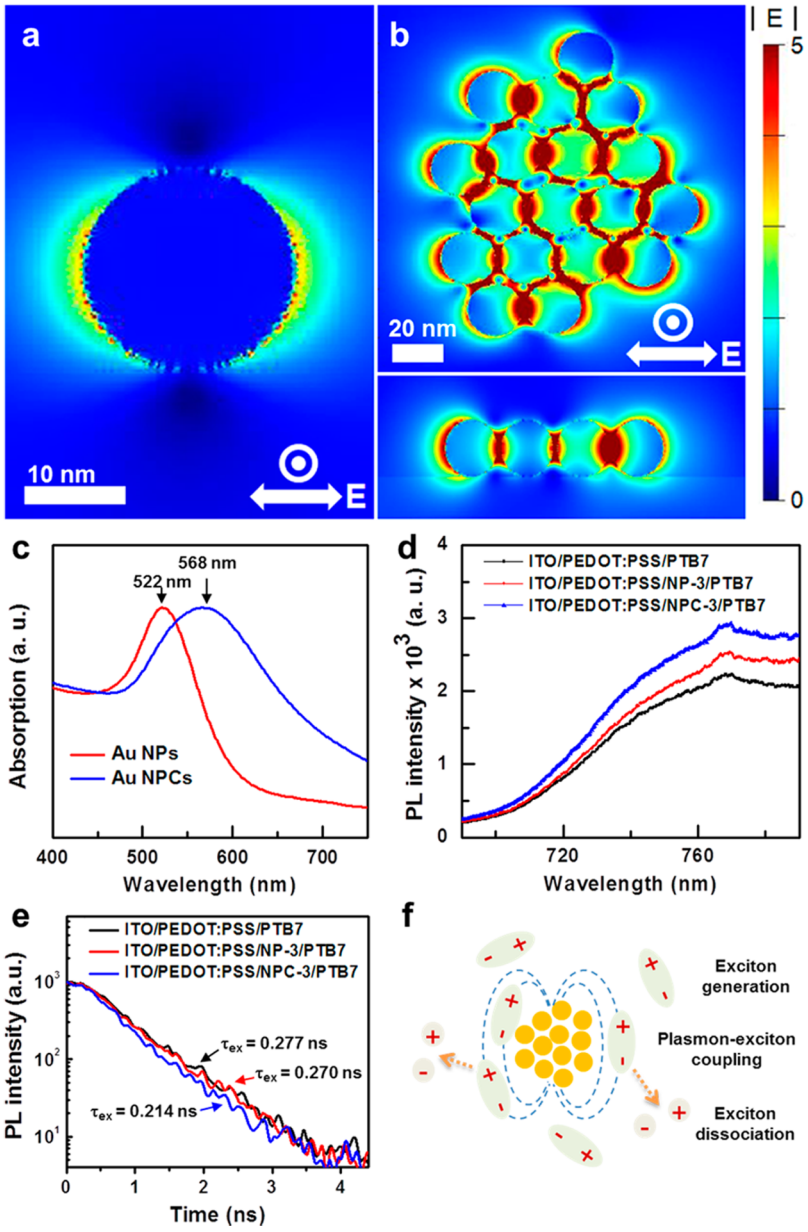

Figure 2. FDTD-simulated electric field distribution of (a) single Au NP and (b) Au NPC. (c) UV−vis absorption spectra of Au NPs and NPCs. (d) Steady-state photoluminescence spectra and (e) photoluminescence decay profile of PTB7 films with and without Au NPs or NPCs. (f) Schematic diagram of the plasmonic effect of Au NPCs.

enhancement, NPCs could be inserted at the interface. NPCs finely dispersed in ethanol could be uniformly deposited on the PEDOT:PSS layer by spin-casting, maintaining their triangular shape (inset of Figure 1e). Subsequently, active materials dissolved in chlorobenzene were deposited by spin-coating. Owing to the solvent orthogonality, NPCs could be embedded in the organic active layer without any damage to their own shape, as shown in Figure 1e. In addition, no significant fluctuation in the thickness of the active layer was observed with bottom NPCs.

Plasmonic characteristics of Au NPC and uncoupled Au NP (mean diameter: 21 nm) were compared by simulation of electric field distribution using finite-difference time domain (FDTD) method. Figure 2a,b contrasts the FDTD-simulated electric field distributions at Au NP and NPC. The excitation wavelength of 685 nm was used in the simulation, which is the maximum absorption peak position of the PTB7 based organic active layer. Owing to the near-field coupling among the closely packed NPs (0.5−2 nm spacing), NPC demonstrates strong enhancement of electric field intensity not only at the gap between individual Au NPs but also at the outer surface. Notably, the maximum field intensity at NPC is about 200-fold enhanced from that of NP. In addition, NPC exhibits different light absorption behavior from NPs. As shown in Figure 2c, UV−vis extinction spectrum of the NPC dispersion in ethanol exhibited a surface plasmon resonance (SPR) peak at 568 nm, which was

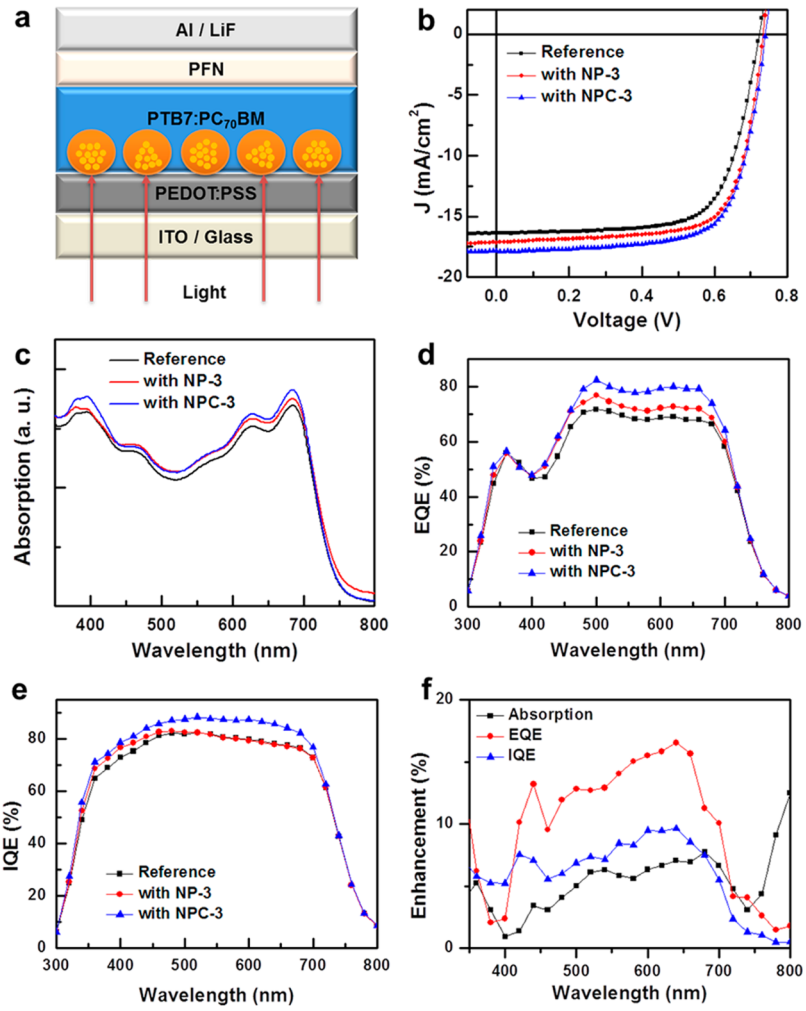

Figure 3. (a) Device structure of OPVs with Au NPCs. (b) *J*–*V* characteristics of OPVs, (c) UV–vis absorption spectra of PTB7:$PC_{70}BM$ film, (d) EQE, and (e) IQE spectra of OPVs with and without Au NPs or NPCs. (f) Percentage enhancement of the absorption, EQE, and IQE values of the device with Au NPCs.

significantly red-shifted and much broader than that of NP dispersion.[61]

Influence from NP and NPC on the optoelectronic properties of PTB7 was investigated by the steady-state and time-resolved photoluminescence (PL) measurements. The steady-state PL spectra of PEDOT:PSS/PTB7, PEDOT:PSS/Au NPs/PTB7, and PEDOT:PSS/Au NPCs/PTB7 films are compared in Figure 2d. The films with NPs or NPCs showed higher PL intensities than pure PTB7 film, confirming that the plasmonic components indeed enhance the exciton generation of PTB7. Significantly, the PL intensity with NPCs is considerably higher than that with NPs. The strong interparticle enhancement of electromagnetic field at NPCs could effectively enhance the exciton generation, as demonstrated by FDTD simulation above. Since NPCs are in direct contact with the PTB7 film in our OPV device structure, the enhanced local electric field may readily influence the photoactive polymers in the vicinity of NPCs. Figure 2e compares the PL intensity decay profiles measured by time-resolved PL. The exciton lifetimes (τ_{ex}) for PEDOT:PSS/PTB7 film and PEDOT:PSS/Au NPs/PTB7 film were 0.277 and 0.270 ns, respectively, signifying that NPs shows no considerable effect on the dissociation of photogenerated excitons. By contrast, the τ_{ex} for PEDOT:PSS/Au NPCs/PTB7 film was 0.214 ns, significantly lower than those for other films. The strong local electromagnetic field around NPCs can more effectively interact with photogenerated excitons in the neighboring photoactive polymers, as depicted in Figure 2f. Such a plasmon–exciton coupling can accelerate exciton dissociation[62] and result in a more efficient charge transfer and shorter τ_{ex}.

We fabricated PTB7-based OPVs, as illustrated in Figure 3a. Alcohol-soluble conjugated polyelectrolyte, poly[(9,9-bis(3′-(N,N-dimethylamino)propyl)-2,7-fluorene)-*alt*-2,7-(9,9-dioctylfluorene)] (PFN), was employed as the electron transport layer.[15] Areal density of the NPCs located at the interface between PEDOT:PSS layer and active layer was controlled by the number of repeated spin-coating. Low coverage (NPC-1, 1.0×10^7 cm^{-2}), medium coverage (NPC-3, 2.9×10^7 cm^{-2}), and high

TABLE 1. Device Characteristics of OPVs with Au NPs and NPCs with Different Areal Densities

NPs/NPCs	V_{oc} [V]	J_{sc} [mA cm^{-2}]	FF [%]	R_sA [Ω cm^{-2}]	R_pA [Ω cm^{-2}]	PCE [%]
reference	0.72	16.39	70.1	5.5	1558.7	8.29
NP-1	0.73	16.58	70.7	5.2	1180.1	8.63
NP-3	0.73	17.04	71.8	4.5	1422.5	8.98
NP-5	0.73	16.80	69.7	5.2	863.6	8.60
NPC-1	0.73	17.35	72.5	4.1	1277.7	9.14
NPC-3	0.73	17.75	73.3	3.5	1573.1	9.48
NPC-5	0.73	17.68	70.6	4.3	1040.6	9.24

coverage (NPC-5, 5.6×10^7 cm^{-2}) of Au NPC layers were prepared by 1, 3, and 5 times of spin-coatings, respectively. Devices with Au NPs were also prepared by similar procedure. The device characteristics of all prepared OPVs are summarized in Table 1 and Supporting Information Figure S1. Figure 3b compares the current density−voltage (J−V) characteristics of the NP-3 and NPC-3 devices and the reference device without plasmonic component. The reference exhibits the open-circuit voltage (V_{oc}) of 0.72 V, short-circuit current density (J_{sc}) of 16.39 mA cm^{-2}, fill factor (FF) of 70.1%, and PCE of 8.29%. For NP-3 device, PCE was increased up to 8.98%, principally due to the J_{sc} improvement to 17.04 mA cm^{-2} and the FF to 71.8%. Notably, NPC-3 device showed the highest J_{sc} of 17.75 mA cm^{-2} and FF of 73.3%, resulting in the PCE of 9.48%. This remarkable enhancement in the device performance is attributed to the synergistic improvement of exciton generation and dissociation caused by strong LSPR at NPCs. Subsequently, NPC-3 device showed a decrease of series resistance (R_s) from 5.5 Ω cm^2 (reference device) to 3.5 Ω cm^2 and relevant FF enhancement. The charge transport behavior with or without NPCs was characterized by the hole mobility measurements of PTB7-based hole-only devices by using space charge limited current (SCLC) model (Supporting Information Figure S2 and Table S1).[63] The device with NPCs showed a considerable increase of hole mobility from 3.30×10^{-4} to 4.90×10^{-4} cm^2 V^{-1} s^{-1}. This additional advantage from NPC incorporation could stem from the effective enhancement of interfacial area between active organic layer and hole transport layer by introducing NPCs with well-matching energy level.[48]

To further elucidate the J_{sc} enhancement with plasmonic components, UV−vis absorption spectra of the organic active layers (Figure 3c), and the external quantum efficiency (EQE) spectra of OPV devices (Figure 3d) are compared. While the light absorption of active layer was enhanced over a broad range from 400 to 700 nm with NPs and NPCs, it exhibits more pronounced improvement from 600 to 700 nm with NPCs (Figure 3c). This behavior is consistent with the UV−vis extinction spectra of the solution dispersions of pure NPs or NPCs presented in Figure 2c. The EQE

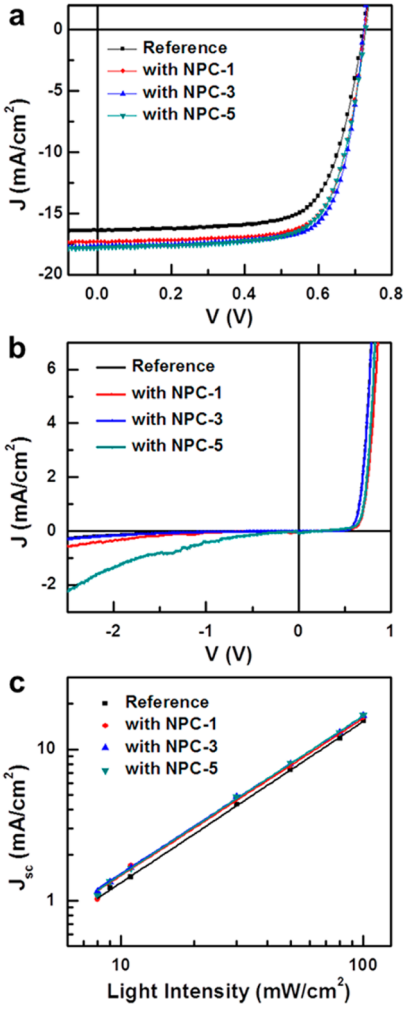

Figure 4. J−V characteristics of OPVs (a) under illumination and (b) under dark condition with different areal densities of Au NPCs. (c) J_{sc} at various light intensities of OPVs with different areal densities of Au NPCs.

spectra also follow similar enhancement behaviors, as shown in Figure 3d. The device with NPCs exhibits the highest improvement in EQE particularly from 500 to 700 nm with the maximum EQE value of 82.4%. The maximum EQE values for the reference and the device with NPs are 71.8% and 76.8%, respectively. The measured EQE enhancements are consistent with the increased J_{sc} values of the OPVs with plasmonic components.

We also analyzed the internal quantum efficiency (IQE) spectra to investigate on the charge carrier collection of OPV devices with plamonic components. The IQE spectra in Figure 3e reveal the enhancement over a broad wavelength range with NPCs, whereas NPs show no significant influence. The maximum IQE values are 82.3%, 83.1%, and 88.4% for the reference device and the device with NPs and NPCs, respectively. The enhancement of IQE indicates a more efficient charge collection from the same number of photogenerated excitons, which should result from the improved exciton dissociation by strong LSPR field

around NPCs. Figure 3f summarizes the percentage enhancement in the absorption, EQE and IQE values of the device with NPCs from reference device without plasmonic component. Strong concurrent enhancements of light absorption and IQE from 500 to 700 nm result in the overall ~17% enhancement of EQE. It is noteworthy that the absorption enhancement is relatively weak over 400−500 nm, where IQE enhancement compensates to result in the EQE enhancement over entire visible range. Taken together, simultaneous improvements of EQE and IQE verify that NPCs with LSPR not only enhance the light absorption but also greatly improve the exciton dissociation in the active layer of OPVs.

Figure 4a illustrates $J-V$ characteristics of the OPVs with different areal densities of NPCs at active layer/hole transport layer interfaces. While all devices with NPCs exhibited improved PCE over 9% (Table 1), NPC-3 device with medium coverage shows the highest PCE. The relatively low PCE of NPC-1 is due to the weak plasmonic effect in the presence of small amount of NPCs, which can also explain the low J_{sc} of NP-1. By contrast, NPC-5 device shows a low FF in comparison to other devices, which could be understood by additional experiments as follows. Diode characteristic measurements under dark condition (Figure 4b) revealed the considerable leakage current of NPC-5 device at reverse bias, presumably caused by the aggregated NPCs of feature size over 200 nm formed during repeated spin-coating. Such aggregation may build-up short circuiting paths within the thin active layer (Supporting Information Figure S3). In addition, J_{sc} measurements at various light intensities (Figure 4c) illustrate the dependence of J_{sc} on illumination intensity of OPVs with various NPC compositions. All fitted curves showed similar slopes with the power factors of 1.03−1.06. This confirms that NPC does not increase charge trap or recombination and, therefore, the reduced FF value of NPC-5 device should be due to leakage current.

CONCLUSIONS

We have presented remarkable performance enhancement of OPVs by employing plasmonic NPCs. A strong enhancement of LSPR field at NPCs is induced by near-field plasmonic coupling and greatly improved the exciton generation and efficient exciton dissociation in the organic active layer consisting of PTB7/PCBM bulkheterojunction. Direct incorporation of NPCs at the bottom of organic active layer improved the PCE from 8.29 to 9.48%. Significantly, this is the first report for the performance enhancement of OPVs by using plasmonic metal NP assembly with controlled morphology. The solution processability of metal NP assemblies is compatible to conventional low-cost OPV process. Moreover, this approach can be further exploited by tuning the shape, dimension and chemical composition of assemblies, the size of constituting NPs, and the interparticle gaps. We anticipate that our approach can be extended to various optoelectronic devices with judicious optimization of plasmonic properties for different device systems.

EXPERIMENTAL METHODS

Synthesis of AuNPs. Spherical Au NPs were prepared as described elsewhere.[64] A volume of 100 mL of $HAuCl_4 \cdot 3H_2O$ (1 mM) was heated to 100 °C under vigorous stirring in a 250 mL round-bottom flask. Ten milliliters of sodium citrate (38.8 mM) was injected to this solution. The reaction mixture was further heated for 10 min, and cooled to room temperature under stirring.

Au NPC Synthesis. Two milliliters of 10 mg mL^{-1} PVP, 1 mL of trisodium citrate (60 mM), and 1 mL of deionized water were mixed in a glass vial at room temperature. Then, 0.1 mL of $HAuCl_4$ (10 mM) and 0.02 mL of KI (50 mM) were added into the reaction mixture. Subsequently, 0.2 mL of H_2O_2 (200 mM), 0.1 mL of AA (100 mM), and 0.2 mL of Ag nanoprism solution were injected. The resultant Au NPCs were thoroughly washed and collected by centrifugation at 3400 rpm with ethanol three times.

OPV Fabrication. PEDOT:PSS (Clevios P VP AI 4083) was deposited by spin-casting at 3500 rpm onto cleaned ITO-coated glass substrates (after UVO irradiation for 20 min) and dried for 20 min at 150 °C. On the PEDOT:PSS layers, Au NPs and NPCs dispersions in ethanol (1 wt %) were spin-cast at 2000 rpm and dried for 3 min at 50 °C. Organic active layers consisting of the blends of PTB7 (1-materials) and $PC_{70}BM$ (1-materials) (25 mg mL^{-1}, 1:1.5 w/w) were spin coated over the Au NP or NPC layer from the solution in chlorobenzene:1,8-diiodooctane (97:3 v/v) by spin-casting at 1000 rpm in a N_2-filled glovebox. PFN (1-materials) was dissolved in methanol (2 mg mL^{-1}) with small amount of acetic acid (2 μL ml^{-1}), and spin-coated on the active layer at 4000 rpm. Subsequently, the LiF/Al (0.5 nm/100 nm) cathode was thermally evaporated. The effective active area of the unit cell was controlled to be 0.12 cm^2. The performance of the devices was tested under AM 1.5G irradiation (100 mW cm^{-2}) with a xenon-lamp solar simulator (Oriel Sol-1A).

Characterization. Morphologies of Au NPs and NPCs were characterized with field-emission SEM (FEI-INSPECT F50) and TEM (Tecnai F20, at 200 kV or a FEI Tecnai TF30 Super-Twin TEM operating at 300 kV). TEM samples were prepared by drop casting on carbon-coated Cu grids (300 mesh). The extinction spectra of AuNP and AuNPC were obtained using an UV−vis-NIR absorption spectrometer (Shimadzu UV-3600).

FDTD Simulation. Electromagnetic field distributions of the AuNP and AuNPC were simulated by the three-dimensional FDTD method[65] with the commercial FDTD-Lumerical simulation package. The refractive index of PTB7:$PC_{70}BM$ film was estimated using spectroscopic ellipsometer (Woollam). The electromagnetic field distribution was then obtained with the mesh size of 0.1 nm at the excitation wavelength of λ_{ex} = 685 nm. The FDTD model for Au NPC was constructed based on the experimentally observed structural parameters.

Conflict of Interest: The authors declare no competing financial interest.

Acknowledgment. This work was financially supported by the Institute for Basic Science (IBS) [IBS-R004-G1-2014-a00]. S.L. and S.W.H. acknowledge the partial financial support from Basic Science Research Programs (2010-0029149) through the NRF funded by the Korea government (MSIP).

Supporting Information Available: Error bars of device characteristics, *J*–*V* characteristics of hole-only devices, hole mobilities of PTB7-based hole-only devices with Au NPCs, cross-sectional SEM image of Si/PEDOT:PSS/NPC-5/PTB7:$PC_{70}BM$ layer, detailed description of quantum efficiency. This material is available free of charge *via* the Internet at http://pubs.acs.org.

REFERENCES AND NOTES

1. Yu, G.; Gao, J.; Hummelen, J. C.; Wudl, F.; Heeger, A. J. Polymer Photovoltaic Cells—Enhanced Efficiencies *via* a Network of Internal Donor-Acceptor Heterojunctions. *Science* **1995**, *270*, 1789–1791.
2. Ma, W. L.; Yang, C. Y.; Gong, X.; Lee, K.; Heeger, A. J. Thermally Stable, Efficient Polymer Solar Cells with Nanoscale Control of the Interpenetrating Network Morphology. *Adv. Funct. Mater.* **2005**, *15*, 1617–1622.
3. Kim, Y.; Cook, S.; Tuladhar, S. M.; Choulis, S. A.; Nelson, J.; Durrant, J. R.; Bradley, D. D. C.; Giles, M.; McCulloch, I.; Ha, C.-S.; *et al.* A Strong Regioregularity Effect in Self-Organizing Conjugated Polymer Films and High-Efficiency Polythiophene:Fullerene Solar Cells. *Nat. Mater.* **2006**, *5*, 197–203.
4. Gunes, S.; Neugebauer, H.; Sariciftci, N. S. Conjugated Polymer-Based Organic Solar Cells. *Chem. Rev.* **2007**, *107*, 1324–1338.
5. Li, G.; Zhu, R.; Yang, Y. Polymer Solar Cells. *Nat. Photonics* **2012**, *6*, 153–161.
6. Liang, Y. Y.; Feng, D. Q.; Wu, Y.; Tsai, S. T.; Li, G.; Ray, C.; Yu, L. P. Highly Efficient Solar Cell Polymers Developed *via* Fine-Tuning of Structural and Electronic Properties. *J. Am. Chem. Soc.* **2009**, *131*, 7792–7799.
7. Chen, H.-Y.; Hou, J.; Zhang, S.; Liang, Y.; Yang, G.; Yang, Y.; Yu, L.; Wu, Y.; Li, G. Polymer Solar Cells with Enhanced Open-Circuit Voltage and Efficiency. *Nat. Photonics* **2009**, *3*, 649–653.
8. Liang, Y.; Xu, Z.; Xia, J.; Tsai, S. T.; Wu, Y.; Li, G.; Ray, C.; Yu, L. For the Bright Future-Bulk Heterojunction Polymer Solar Cells with Power Conversion Efficiency of 7.4%. *Adv. Mater.* **2010**, *22*, E135–138.
9. Chu, T. Y.; Lu, J.; Beaupre, S.; Zhang, Y.; Pouliot, J. R.; Wakim, S.; Zhou, J.; Leclerc, M.; Li, Z.; Ding, J.; *et al.* Bulk Heterojunction Solar Cells Using Thieno[3,4-*c*]pyrrole-4,6-dione and Dithieno[3,2-*b*:2′,3′-*d*]silole Copolymer with a Power Conversion Efficiency of 7.3%. *J. Am. Chem. Soc.* **2011**, *133*, 4250–4253.
10. Price, S. C.; Stuart, A. C.; Yang, L.; Zhou, H.; You, W. Fluorine Substituted Conjugated Polymer of Medium Band Gap Yields 7% Efficiency in Polymer-Fullerene Solar Cells. *J. Am. Chem. Soc.* **2011**, *133*, 4625–4631.
11. Huang, Y.; Guo, X.; Liu, F.; Huo, L.; Chen, Y.; Russell, T. P.; Han, C. C.; Li, Y.; Hou, J. Improving the Ordering and Photovoltaic Properties by Extending Pi-Conjugated Area of Electron-Donating Units in Polymers with D-A Structure. *Adv. Mater.* **2012**, *24*, 3383–3389.
12. Dou, L.; Chang, W. H.; Gao, J.; Chen, C. C.; You, J.; Yang, Y. A Selenium-Substituted Low-Bandgap Polymer with Versatile Photovoltaic Applications. *Adv. Mater.* **2013**, *25*, 825–831.
13. Lee, J. M.; Park, J. S.; Lee, S. H.; Kim, H.; Yoo, S.; Kim, S. O. Selective Electron- or Hole-Transport Enhancement in Bulk-Heterojunction Organic Solar Cells with N- or B-Doped Carbon Nanotubes. *Adv. Mater.* **2011**, *23*, 629–633.
14. Lee, J. M.; Kwon, B. H.; Park, H. I.; Kim, H.; Kim, M. G.; Park, J. S.; Kim, E. S.; Yoo, S.; Jeon, D. Y.; Kim, S. O. Exciton Dissociation and Charge-Transport Enhancement in Organic Solar Cells with Quantum-Dot/N-Doped CNT Hybrid Nanomaterials. *Adv. Mater.* **2013**, *25*, 2011–2017.
15. He, Z.; Zhong, C.; Su, S.; Xu, M.; Wu, H.; Cao, Y. Enhanced Power-Conversion Efficiency in Polymer Solar Cells Using an Inverted Device Structure. *Nat. Photonics* **2012**, *6*, 593–597.
16. Leem, D. S.; Edwards, A.; Faist, M.; Nelson, J.; Bradley, D. D. C.; de Mello, J. C. Efficient Organic Solar Cells with Solution-Processed Silver Nanowire Electrodes. *Adv. Mater.* **2011**, *23*, 4371–4375.
17. Lu, L.; Xu, T.; Chen, W.; Lee, J. M.; Luo, Z.; Jung, I. H.; Park, H. I.; Kim, S. O.; Yu, L. The Role of N-Doped Multiwall Carbon Nanotubes in Achieving Highly Efficient Polymer Bulk Heterojunction Solar Cells. *Nano Lett.* **2013**, *13*, 2365–2369.
18. He, Z. C.; Zhong, C. M.; Huang, X.; Wong, W. Y.; Wu, H. B.; Chen, L. W.; Su, S. J.; Cao, Y. Simultaneous Enhancement of Open-Circuit Voltage, Short-Circuit Current Density, and Fill Factor in Polymer Solar Cells. *Adv. Mater.* **2011**, *23*, 4636–4643.
19. He, Z. C.; Zhang, C.; Xu, X. F.; Zhang, L. J.; Huang, L.; Chen, J. W.; Wu, H. B.; Cao, Y. Largely Enhanced Efficiency with a PFN/Al Bilayer Cathode in High Efficiency Bulk Heterojunction Photovoltaic Cells with a Low Bandgap Polycarbazole Donor. *Adv. Mater.* **2011**, *23*, 3086–3089.
20. Campoy-Quiles, M.; Ferenczi, T.; Agostinelli, T.; Etchegoin, P. G.; Kim, Y.; Anthopoulos, T. D.; Stavrinou, P. N.; Bradley, D. D.; Nelson, J. Morphology Evolution *via* Self-Organization and Lateral and Vertical Diffusion in Polymer:Fullerene Solar Cell Blends. *Nat. Mater.* **2008**, *7*, 158–164.
21. Choi, M. R.; Han, T. H.; Lim, K. G.; Woo, S. H.; Huh, D. H.; Lee, T. W. Soluble Self-Doped Conducting Polymer Compositions with Tunable Work Function as Hole Injection/Extraction Layers in Organic Optoelectronics. *Angew. Chem., Int. Ed.* **2011**, *50*, 6274–6277.
22. Li, G.; Shrotriya, V.; Huang, J.; Yao, Y.; Moriarty, T.; Emery, K.; Yang, Y. High-Efficiency Solution Processable Polymer Photovoltaic Cells by Self-Organization of Polymer Blends. *Nat. Mater.* **2005**, *4*, 864–868.
23. Kim, J. Y.; Lee, K.; Coates, N. E.; Moses, D.; Nguyen, T. Q.; Dante, M.; Heeger, A. J. Efficient Tandem Polymer Solar Cells Fabricated by All-Solution Processing. *Science* **2007**, *317*, 222–225.
24. Peet, J.; Kim, J. Y.; Coates, N. E.; Ma, W. L.; Moses, D.; Heeger, A. J.; Bazan, G. C. Efficiency Enhancement in Low-Bandgap Polymer Solar Cells by Processing with Alkane Dithiols. *Nat. Mater.* **2007**, *6*, 497–500.
25. You, J.; Chen, C. C.; Hong, Z.; Yoshimura, K.; Ohya, K.; Xu, R.; Ye, S.; Gao, J.; Li, G.; Yang, Y. 10.2% Power Conversion Efficiency Polymer Tandem Solar Cells Consisting of Two Identical Sub-Cells. *Adv. Mater.* **2013**, *25*, 3973–3978.
26. Lee, J. K.; Ma, W. L.; Brabec, C. J.; Yuen, J.; Moon, J. S.; Kim, J. Y.; Lee, K.; Bazan, G. C.; Heeger, A. J. Processing Additives for Improved Efficiency from Bulk Heterojunction Solar Cells. *J. Am. Chem. Soc.* **2008**, *130*, 3619–3623.
27. Li, X.; Choy, W. C.; Huo, L.; Xie, F.; Sha, W. E.; Ding, B.; Guo, X.; Li, Y.; Hou, J.; You, J.; *et al.* Dual Plasmonic Nanostructures for High Performance Inverted Organic Solar Cells. *Adv. Mater.* **2012**, *24*, 3046–3052.
28. He, X.; Gao, F.; Tu, G.; Hasko, D.; Huttner, S.; Steiner, U.; Greenham, N. C.; Friend, R. H.; Huck, W. T. Formation of Nanopatterned Polymer Blends in Photovoltaic Devices. *Nano Lett.* **2010**, *10*, 1302–1307.
29. Service, R. F. Outlook Brightens for Plastic Solar Cells. *Science* **2011**, *332*, 293.
30. Chen, D.; Liu, F.; Wang, C.; Nakahara, A.; Russell, T. P. Bulk Heterojunction Photovoltaic Active Layers *via* Bilayer Interdiffusion. *Nano Lett.* **2011**, *11*, 2071–2078.
31. Ochiai, S.; Kumar, P.; Santhakumar, K.; Shin, P.-K. Examining the Effect of Additives and Thicknesses of Hole Transport Layer for Efficient Organic Solar Cell Devices. *Electron. Mater. Lett.* **2013**, *9*, 399–403.
32. Scharber, M. C.; Mühlbacher, D.; Koppe, M.; Denk, P.; Waldauf, C.; Heeger, A. J.; Brabec, C. J. Design Rules for Donors in Bulk-Heterojunction Solar Cells—Towards 10% Energy-Conversion Efficiency. *Adv. Mater.* **2006**, *18*, 789–794.
33. Forrest, S. R. The Limits to Organic Photovoltaic Cell Efficiency. *MRS Bull.* **2005**, *30*, 28–32.
34. Blom, P. W. M.; Mihailetchi, V. D.; Koster, L. J. A.; Markov, D. E. Device Physics of Polymer:Fullerene Bulk Heterojunction Solar Cells. *Adv. Mater.* **2007**, *19*, 1551–1566.
35. Atwater, H. A.; Polman, A. Plasmonics for Improved Photovoltaic Devices. *Nat. Mater.* **2010**, *9*, 205–213.
36. Lu, L.; Luo, Z.; Xu, T.; Yu, L. Cooperative Plasmonic Effect of Ag and Au Nanoparticles on Enhancing Performance of Polymer Solar Cells. *Nano Lett.* **2013**, *13*, 59–64.

37. Wang, D. H.; Kim do, Y.; Choi, K. W.; Seo, J. H.; Im, S. H.; Park, J. H.; Park, O. O.; Heeger, A. J. Enhancement of Donor-Acceptor Polymer Bulk Heterojunction Solar Cell Power Conversion Efficiencies by Addition of Au Nanoparticles. *Angew. Chem., Int. Ed.* **2011**, *50*, 5519–5523.
38. Wang, D. H.; Park, K. H.; Seo, J. H.; Seifter, J.; Jeon, J. H.; Kim, J. K.; Park, J. H.; Park, O. O.; Heeger, A. J. Enhanced Power Conversion Efficiency in PCDTBT/$PC_{70}BM$ Bulk Heterojunction Photovoltaic Devices with Embedded Silver Nanoparticle Clusters. *Adv. Energy Mater.* **2011**, *1*, 766–770.
39. Baek, S.-W.; Noh, J.; Lee, C.-H.; Kim, B.; Seo, M.-K.; Lee, J.-Y. Plasmonic Forward Scattering Effect in Organic Solar Cells: A Powerful Optical Engineering Method. *Sci. Rep.* **2013**, *3*, 1726.
40. Li, X.; Choy, W. C. H.; Lu, H.; Sha, W. E. I.; Ho, A. H. P. Efficiency Enhancement of Organic Solar Cells by Using Shape-Dependent Broadband Plasmonic Absorption in Metallic Nanoparticles. *Adv. Funct. Mater.* **2013**, *23*, 2728–2735.
41. Choi, H.; Lee, J. P.; Ko, S. J.; Jung, J. W.; Park, H.; Yoo, S.; Park, O.; Jeong, J. R.; Park, S.; Kim, J. Y. Multipositional Silica-Coated Silver Nanoparticles for High-Performance Polymer Solar Cells. *Nano Lett.* **2013**, *13*, 2204–2208.
42. Jageler-Hoheisel, T.; Selzer, F.; Riede, M.; Leo, K. Direct Electrical Evidence of Plasmonic Near-Field Enhancement in Small Molecule Organic Solar Cells. *J. Phys. Chem. C* **2014**, *118*, 15128–15135.
43. Jung, K.; Song, H. J.; Lee, G.; Ko, Y.; Ahn, K.; Choi, H.; Kim, J. Y.; Ha, K.; Song, J.; Lee, J. K.; *et al.* Plasmonic Organic Solar Cells Employing Nanobump Assembly *via* Aerosol-Derived Nanoparticles. *ACS Nano* **2014**, *8*, 2590–2601.
44. Chuang, M. K.; Lin, S. W.; Chen, F. C.; Chu, C. W.; Hsu, C. S. Gold Nanoparticle-Decorated Graphene Oxides for Plasmonic-Enhanced Polymer Photovoltaic Devices. *Nanoscale* **2014**, *6*, 1573–1579.
45. Choi, H.; Ko, S.-J.; Choi, Y.; Joo, P.; Kim, T.; Lee, B. R.; Jung, J.-W.; Choi, H. J.; Cha, M.; Jeong, J.-R.; *et al.* Versatile Surface Plasmon Resonance of Carbon-Dot-Supported Silver Nanoparticles in Polymer Optoelectronic Devices. *Nat. Photonics* **2013**, *7*, 732–738.
46. Gan, Q.; Bartoli, F. J.; Kafafi, Z. H. Plasmonic-Enhanced Organic Photovoltaics: Breaking the 10% Efficiency Barrier. *Adv. Mater.* **2013**, *25*, 2385–2396.
47. Chou, C.-H.; Chen, F.-C. Plasmonic Nanostructures for Light Trapping in Organic Photovoltaic Devices. *Nanoscale* **2014**, *6*, 8444–8458.
48. Wang, C. C. D.; Choy, W. C. H.; Duan, C.; Fung, D. D. S.; Sha, W. E. I.; Xie, F.-X.; Huang, F.; Cao, Y. Optical and Electrical Effects of Gold Nanoparticles in the Active Layer of Polymer Solar Cells. *J. Mater. Chem.* **2012**, *22*, 1206.
49. Yang, J.; You, J. B.; Chen, C. C.; Hsu, W. C.; Tan, H. R.; Zhang, X. W.; Hong, Z. R.; Yang, Y. Plasmonic Polymer Tandem Solar Cell. *ACS Nano* **2011**, *5*, 6210–6217.
50. Wu, J. L.; Chen, F. C.; Hsiao, Y. S.; Chien, F. C.; Chen, P. L.; Kuo, C. H.; Huang, M. H.; Hsu, C. S. Surface Plasmonic Effects of Metallic Nanoparticles on the Performance of Polymer Bulk Heterojunction Solar Cells. *ACS Nano* **2011**, *5*, 959–967.
51. Tan, K. S.; Chuang, M. K.; Chen, F. C.; Hsu, C. S. Solution-Processed Nanocomposites Containing Molybdenum Oxide and Gold Nanoparticles as Anode Buffer Layers in Plasmonic-Enhanced Organic Photovoltaic Devices. *ACS Appl. Mater. Interfaces* **2013**, *5*, 12419–12424.
52. Hutter, E.; Fendler, J. H. Exploitation of Localized Surface Plasmon Resonance. *Adv. Mater.* **2004**, *16*, 1685–1706.
53. Bellessa, J.; Bonnand, C.; Plenet, J.; Mugnier, J. Strong Coupling between Surface Plasmons and Excitons in an Organic Semiconductor. *Phys. Rev. Lett.* **2004**, *93*, 036404.
54. Sugawara, Y.; Kelf, T.; Baumberg, J.; Abdelsalam, M.; Bartlett, P. Strong Coupling between Localized Plasmons and Organic Excitons in Metal Nanovoids. *Phys. Rev. Lett.* **2006**, *97*, 266808.
55. Kulkarni, A. P.; Noone, K. M.; Munechika, K.; Guyer, S. R.; Ginger, D. S. Plasmon-Enhanced Charge Carrier Generation in Organic Photovoltaic Films Using Silver Nanoprisms. *Nano Lett.* **2010**, *10*, 1501–1505.
56. Fofang, N. T.; Grady, N. K.; Fan, Z.; Govorov, A. O.; Halas, N. J. Plexciton Dynamics: Exciton-Plasmon Coupling in a J-Aggregate-Au Nanoshell Complex Provides a Mechanism for Nonlinearity. *Nano Lett.* **2011**, *11*, 1556–1560.
57. Manjavacas, A.; Garcia de Abajo, F. J.; Nordlander, P. Quantum Plexcitonics: Strongly Interacting Plasmons and Excitons. *Nano Lett.* **2011**, *11*, 2318–2323.
58. Kumar, A.; Srivastava, R.; Tyagi, P.; Mehta, D. S.; Kamalasanan, M. N. Efficiency Enhancement of Organic Light Emitting Diode *via* Surface Energy Transfer between Exciton and Surface Plasmon. *Org. Electron.* **2012**, *13*, 159–165.
59. Ostrowski, J. C.; Mikhailovsky, A.; Bussian, D. A.; Summers, M. A.; Buratto, S. K.; Bazan, G. C. Enhancement of Phosphorescence by Surface-Plasmon Resonances in Colloidal Metal Nanoparticles: The Role of Aggregates. *Adv. Funct. Mater.* **2006**, *16*, 1221–1227.
60. Lee, S.; Hong, J. W.; Lee, S.-U.; Lee, Y. W.; Han, S. W. Facile Synthesis of Au Nanoparticle Clusters by Using Ag Nanoparticles as Sacrificial Templates for Efficient Surface-Enhanced Raman Scattering Platforms. *Angew. Chem., Int. Ed.*, submitted for publication, **2014**.
61. Halas, N. J.; Lal, S.; Chang, W. S.; Link, S.; Nordlander, P. Plasmons in Strongly Coupled Metallic Nanostructures. *Chem. Rev.* **2011**, *111*, 3913–3961.
62. Moet, D. J. D.; Lenes, M.; Morana, M.; Azimi, H.; Brabec, C. J.; Blom, P. W. M. Enhanced Dissociation of Charge-Transfer States in Narrow Band Gap Polymer:Fullerene Solar Cells Processed with 1,8-Octanedithiol. *Appl. Phys. Lett.* **2010**, *96*, 213506.
63. Mihailetchi, V. D.; Xie, H. X.; de Boer, B.; Koster, L. J. A.; Blom, P. W. M. Charge Transport and Photocurrent Generation in Poly(3-hexylthiophene):Methanofullerene Bulk-Heterojunction Solar Cells. *Adv. Funct. Mater.* **2006**, *16*, 699–708.
64. Grabar, K. C.; Freeman, R. G.; Hommer, M. B.; Natan, M. J. Preparation and Characterization of Au Colloid Monolayers. *Anal. Chem.* **1995**, *67*, 735–743.
65. Oubre, C.; Nordlander, P. Optical Properties of Metallodielectric Nanostructures Calculated Using the Finite Difference Time Domain Method. *J. Phys. Chem. B* **2004**, *108*, 17740–17747.